

# *Preliminary investigation into metal-material extrusion*

**Shane Terry, Ismail Fidan & Khalid Tantawi**

**Progress in Additive Manufacturing**

ISSN 2363-9512

Prog Addit Manuf

DOI 10.1007/s40964-020-00151-5



**Your article is protected by copyright and all rights are held exclusively by Springer Nature Switzerland AG. This e-offprint is for personal use only and shall not be self-archived in electronic repositories. If you wish to self-archive your article, please use the accepted manuscript version for posting on your own website. You may further deposit the accepted manuscript version in any repository, provided it is only made publicly available 12 months after official publication or later and provided acknowledgement is given to the original source of publication and a link is inserted to the published article on Springer's website. The link must be accompanied by the following text: "The final publication is available at [link.springer.com](http://link.springer.com)".**



# Preliminary investigation into metal-material extrusion

Shane Terry<sup>1</sup> · Ismail Fidan<sup>2</sup> · Khalid Tantawi<sup>3</sup>Received: 23 November 2019 / Accepted: 14 September 2020  
© Springer Nature Switzerland AG 2020

## Abstract

Additive manufacturing (AM) technologies provide a method of fabrication that minimizes the production of waste and maximizes part customization. The most common form of this technology is material extrusion (ME) in which material is deposited layer-by-layer to produce a highly customized part. However, this additive production method has experienced difficulty in widespread adoption in metal fabrication due to the inability to produce metallic parts with strong mechanical properties. This study presents some innovations on a new metal-fabrication technique for ME printing that allows for low-cost metal printing. A metal powder polymer composite filament, with a high metal composition, can be printed and sintered to yield a part that is completely metal. Overall, this study provides the initial investigation of the microstructural behavior and the resulting hardness levels. This study found that the metal powder in finished parts is fused by approximately 90% derived from the percent area porosity on a microstructural level. The final hardness of the processed parts is reduced by approximately 60%. Characterizing these properties is the initial step in incorporating ME technology in the field of metal 3D printing.

**Keywords** Additive manufacturing · Metal 3D printing · Metal material extrusion · Microstructure · Hardness · Copper

## 1 Introduction

Additive manufacturing (AM) encompasses a variety of fabrication technologies such as powder bed fusion (PBF), vat polymerization, and material extrusion (ME) [1]. The most commonly utilized method is ME in which a material filament is fed into the extrusion system and heated near the melting temperature of the polymer. The end effector will feed and fuse the new layer of material to the previous one.

The overall ME process of forming parts through layered material extrusion is demonstrated in Fig. 1 [2]. By fabricating metal parts via ME, the ease of operation, safety, and waste reduction are all greatly improved. This unique form of fabrication has allowed for opportunities in biological [3], automotive [4], construction [6, 7], and aerospace printing [7]. One area that is under-researched in AM, especially in comparison to other forms of metal 3D printing (M3DP), is metal ME (MME).

Common methods of metal printing are laser sintering (LS), electron beam melting (EBM), and direct metal deposition (DMD). These techniques are expensive, present safety concerns, and require a large operational footprint. Utilizing ME technology, the aforementioned disadvantages can be mitigated to produce relatively inexpensive metal parts within a unique research area that is narrowly studied [8, 9]. This method involves fusing a polymer matrix and metal powder to produce a filament that is denoted as a metal polymer composite (MPC). The objective of the research presented here is to demonstrate the validity of printing metal through the material extrusion process. The overall density of the MPC material is comprised of both metal powders and a polymer matrix which correlates to an expected higher porosity in the finished

✉ Ismail Fidan  
IFidan@tntech.edu

Shane Terry  
SMTerry42@students.tntech.edu

Khalid Tantawi  
Khalid-Tantawi@utc.edu

<sup>1</sup> Department of Mechanical Engineering and Center for Manufacturing Research, College of Engineering, Tennessee Technological University, Cookeville, USA

<sup>2</sup> Department of Manufacturing and Engineering Technology, College of Engineering, Tennessee Technological University, Cookeville, USA

<sup>3</sup> Department of Engineering Management and Technology, University of Tennessee at Chattanooga, Chattanooga, USA

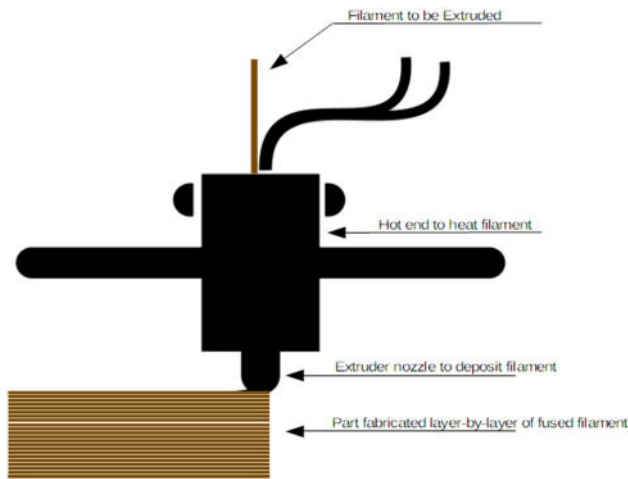


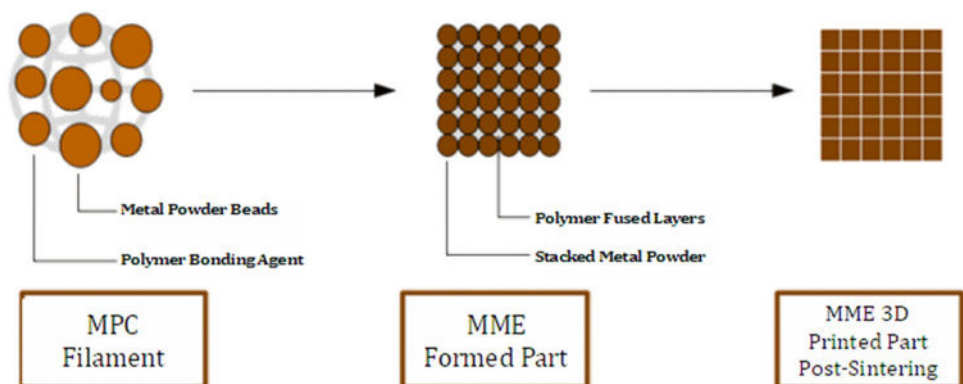
**Fig. 1** The ME process deposits primed material layer-by-layer to build up a 3D object

part versus other metal powder printing techniques that do not rely on the polymer matrix. The results objective is to determine the feasibility of MME as a process, and in line with these objectives microstructure and hardness analyses are performed.

The demonstrative view of the MPC material used for this study is shown in Fig. 2. This graphic illustrates the formation of the metal bead structure pre- and post-printing. The metal is scattered randomly throughout the filament and is more uniformly distributed after printing. Following the sintering procedure, the metal powder melts and fuses together to yield a metal formed object.

This high metal composition filament is printable because of the base polymer which is described as a PLA-compliant material. As such, the MPC filament prints similarly to PLA feedstock with some changes necessary to print properly. The finalized object can then be sintered to produce a 100% metal part. The experimental setup and overall process of MME using MPC material is demonstrated in Fig. 3.

**Fig. 2** Demonstration of the MME procedure in a step-wise manner, and the overall metal powder bead behavior through the process



MME is defined by the following procedure:

- The metal composite filament is preheated during the printing procedure to increase ductility.
- The MPC material is printed on an ME printer at reduced speed and increased material flow.
- Printed specimens are suspended in a sintering ballast to reduced oxidation.
- The temperature sweep passes through specific set points to properly bond the metal and remove the polymer bonding agent.

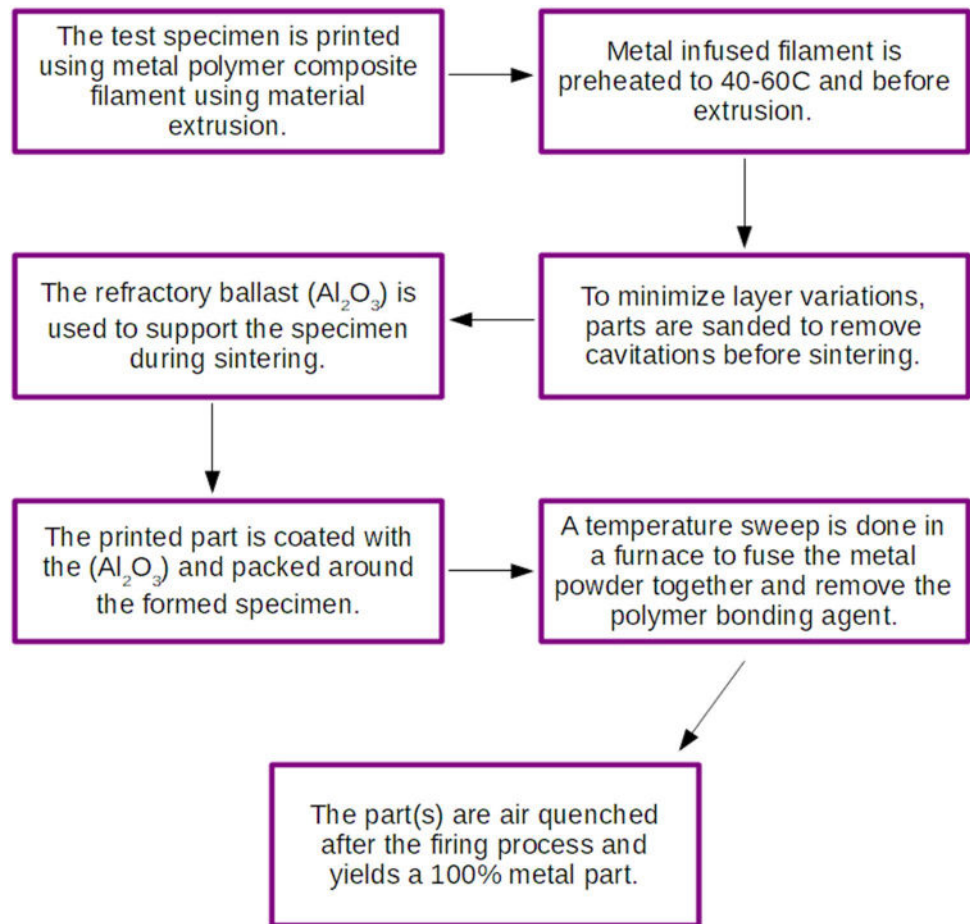
To properly characterize this fabrication technique, the microstructure, dimensional accuracy, and material properties must be understood, which is the goal of this study.

## 2 Background

There are numerous studies that have investigated the field of M3DP and the applications, fabrication methods, materials, and overall technology. M3DP is most utilized in the field of aerospace where the weight reduction and customization that the technique affords cannot be fabricated by any other method [10, 11].

The mechanical behavior of M3DP techniques is compared to MME. It is found that the common M3DP techniques have processing defects that result in a loss of maximum stress that the fabricated parts can withstand reducing mechanical strength. Furthermore, these processes are also shown to be time-consuming and expensive [12]. The business case assessment will ultimately determine the success of AM as it is currently favored in smaller production lots. The higher cost of raw materials is offset by lower fixed costs related to conventional manufacturing. However, there is a large value to be put on AM due to the versatility and adaptability of the process. Overall, AM is projected to lead to new advancements in manufacturing components and will continue to grow with technology [13].

**Fig. 3** Demonstration of the experimental setup and MME fabrication process



Commercially available metal 3D printers commonly utilize the processes of laser sintering (LS) and DMD instead of ME. LS and DMD have previously been examined and compared to other powder metallurgy (PM) techniques [14]. The research group from the Singapore Centre for 3D printing found that LS is a more applicable choice for fabricated parts that require complex geometric internal structures and cavitations. DMD is able to produce larger parts at the expense of dimensional accuracy and can serve as an alternative to the fabrication of large-scale components. Another recent study further compared MME fabrication to LS. The two innovative technologies have different benefits, requirements, and strengths [9].

Indirect metal fabrication is the primary method of utilizing ME technology in the field of M3DP. Parts printed in 3D can be used to generate a casting mold, indirectly forming patterns and sand-formed metal objects [15, 16]. These techniques encompass all of the expenses and safety requirements associated with casting used to fabricate parts.

The relevancy of ME to metal is perceived to be low in a literature review of M3DP. Duda et al. published a literature study on the many forms of M3DP techniques, outlining the benefits and drawbacks of each method [17].

The work done by the research group provides general and design information on AM technologies and their relevancy to metal fabrication. The group compared the various processes in relation to material, labor, and energy costs, and concluded that ME is not relevant to the field of M3DP. The study of MME presented in this paper shows that the AM method of ME should be considered relevant to the field of M3DP counter to Pentair's research [17].

MME was initially studied in 2016 by sintering a metal-filled filament to yield a 100% metal object. Riecker et al. produced their own polymer composite material by infusing a polyamide nylon (PA) matrix with a metal powder filling [8]. The weight percent of the metal polymer composition varied between 0 and 65%. The filament created had brittle mechanical properties and was sintered to remove the bonding agent [8]. Moreover, Hwang et al. found a method of infusing acrylonitrile butadiene styrene (ABS) with copper and iron powder to form a MPC material [18]. The metal content varied from 10 to 50% by weight. The results of this study showed that tensile strength decreased with the introduction of metal powders but thermal conductivity increased.

The field of metal fabrication by ME has been explored by both hobbyist and commercial communities, but it has scarcely been investigated in research and development. Few studies examine the concept of sintering ME objects to yield a 100% metal part, presenting an opportunity in low-cost M3DP characterization [8, 9].

### 3 Methodology and output

#### 3.1 Procedure for specimen fabrication

The material utilized for this study, as previously described, is a MPC, which will be defined as MPC. For this study, the filament has metal inclusions of copper powder along with the polymer matrix. This material is obtained from virtual foundry which has a stated metal composition of 90% by weight [19]. As mentioned in the introduction, the printing procedure for the MPC material is most similar to the base polymer a PLA-compliant filament. Along with the changes detailed later in Table 1, the printing temperature must be set a little higher at 220 °C and the printer nozzle diameter must be larger to compensate for the particle inclusions. Once printed, the MPC specimen is then sintered, resulting in a 100% metal part that retains the original features of the 3D printed object. For the printing procedure, a standard ME printer is used to fabricate with the MPC material. An induction furnace is used to sinter the material in an open-air environment. The final procedure is the post-processing of the sintered specimens to remove oxides and contaminants. MME As demonstrated previously in Fig. 2, the metal powder behavior throughout the MME process is that it is randomly scattered in the filament and is distributed more consistently throughout the formed part. The details and magnified visualization of the material used is shown in Fig. 4.

**Table 1** Description of the labelling nomenclature for the changed variables for dimensional and microstructural analysis of copper

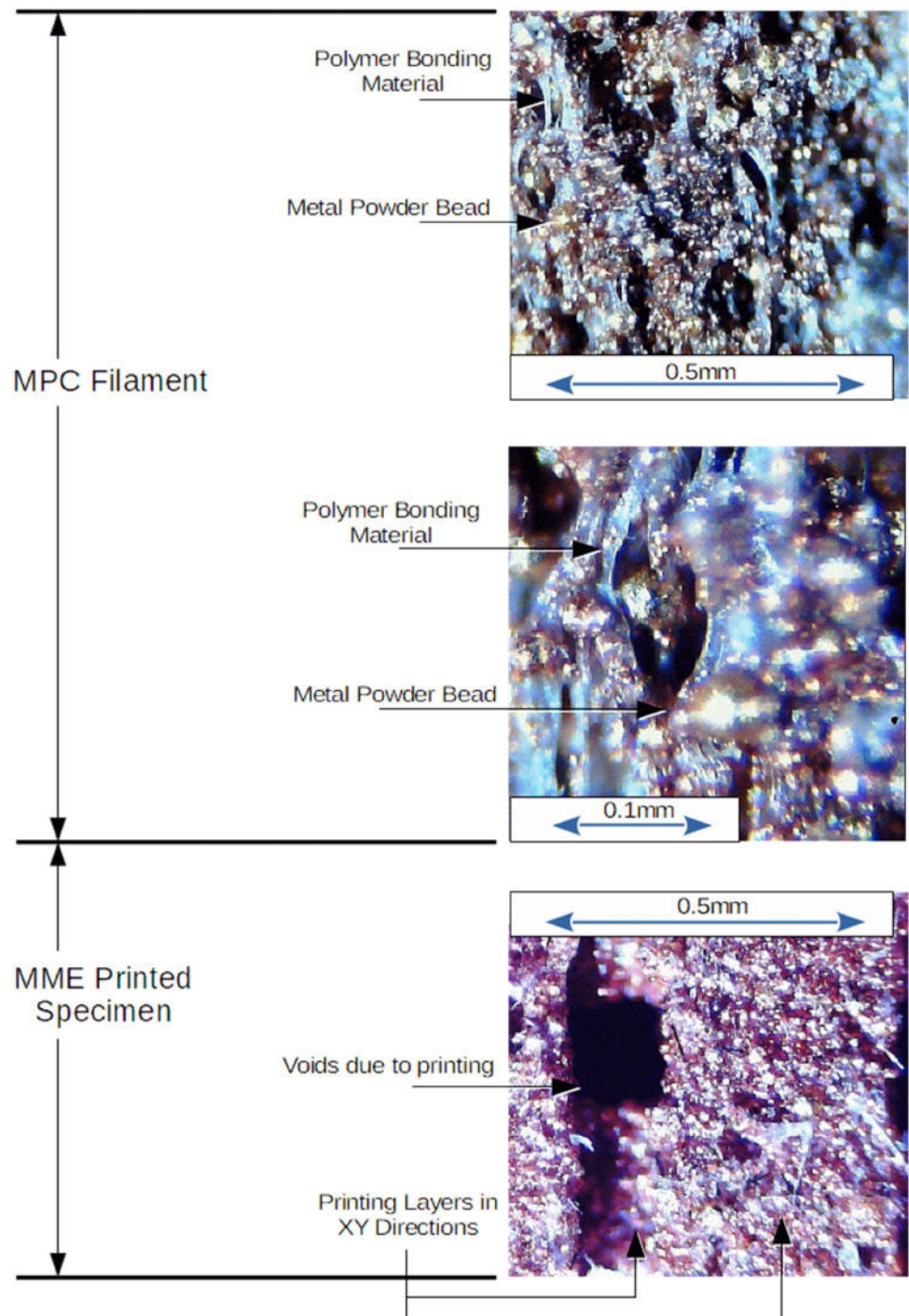
General specimen labels given in the form: CU·L <sub>H</sub> ·S <sub>p</sub> ·V	
Material	
CU	Copper filament
Layer height (L <sub>H</sub> )	
03	0.3 mm
0225	0.225 mm
015	0.15 mm
Print speed (S <sub>p</sub> )	
10	10 mm/s
20	20 mm/s
Specimen size (V)	
V	0.5 in <sup>3</sup>

**MME** The process of using powder-based 3D printing allows for highly complex and customized parts; however, the sintering portion of fabrication involves removing the powder bonding agent. This removal of approximately 10 wt% polymer material results in dimensional changes between the original specimen size and the post-sinter metal samples. To better account for the influence of these changes, a variety of printing parameters are chosen to demonstrate the influence on the MME process. The printing parameters of the specimens are varied to account for the influence of the forming process on the dimensional changes. The printing parameters that are varied for this study are shown in Table 1. These variables are selected based on the most commonly used settings for 3D printing. For all testing performed, the sampled size (*n*) is equal to 3 to account for statistical variations.

The nozzle used for the printing process is stainless steel with a bore hole diameter of 0.6 mm. The layer height (*L<sub>H</sub>*) chosen for this experimental analysis is determined using a combination of professional knowledge of the material extrusion process along with software suggested settings. This knowledge is applied in the form of deriving the *L<sub>H</sub>* from the printing orifice. The minimal layer height should not be below 25% of the nozzle bore diameter, and the maximum should be less than 75% of the nozzle bore diameter. Therefore, layer heights within the range of 0.15–0.45 mm are within acceptable values based on the diameter of the nozzle. The default value and most commonly used layer height for most 3D slicing software is 0.2 mm. Taking three values for statistical variability, the layer height of 0.2 ± 0.5% produces the *L<sub>H</sub>* discrete values of [0.1 0.2 0.3] mm. However, the minimum value of *L<sub>H</sub>* based on 0.2 results in a minimum layer height that is less than the advisable value based on nozzle diameter. In exploratory testing, it was found that layer heights of less than 0.15 mm would not print effectively due to metal particles. Therefore, taking the minimally accepted value based on the nozzle diameter of 0.15 mm and a statistical variance of 3 over layer heights to 0.3 mm results in the three discrete *L<sub>H</sub>* values of [0.15, 0.225, 0.3] mm.

For the variable of printing speed (*S<sub>p</sub>*), the term refers to infill, wall, travel, and initial layer speed. For material extrusion of filled filaments, *S<sub>p</sub>* is reduced and the amount of reduction is dependent on the extrusion method and material used. For a Bowden extrusion setup, the distance between the extrusion motor and the heating element is quite large. Therefore, the printing speeds are further reduced for fragile filled filaments. In a preliminary exploration, it was found that speeds greater than 20 mm/s for copper filled filament in a Bowden printing setup would result in voids during the printing process. The values of printing speed are selected as [10, 20] mm/s to establish some variance between 0 and 20 mm/s. The

**Fig. 4** Magnified view of the metal powder behavior pre-sintering in the MPC filament before and after the printing process



aforementioned printing and specimen parameters used for the experimental process are detailed in Table 1. The table further establishes the specimen nomenclature used for the rest of the presentation of the data with specimen labels presented as the following: CU for the copper material,  $L_H$  for the printing layer height,  $S_p$  for the printing speed, and  $V$  for the specimen volume size. This results in specimen labels written in the general form  $CU \cdot L_H \cdot S_p \cdot V$ .

For the sintering process, the ballast that is used to suspend the formed part is  $Al_2O_3$ , and the temperatures and times used for the processing of the copper specimens are detailed in Table 2. These settings are derived from preliminary thermogravimetric analysis of the MPC material used. The full decomposition temperature for the polymer in the filament was  $\sim 350$  °C, and the melting point of copper is  $\sim 1000$  °C. Taking these two values into account, the

**Table 2** Description of the time and temperature sweeps used for the sintering process

Temperature	Time
150 °C	Hold for 75 min
400 °C	Ramp over 200 min at 1.25 °C/min
983 °C	Ramp over 180 min at 3.24 °C/min
983 °C	Hold for 240 min

early exploratory phase of this study found that the times and temperature presented in Table 2 were the most effective in the open-air furnace environment.

During the post-sintering phase, the containments and oxides are removed, and the final resultant cubes are the specimens that will be utilized for the microstructure and hardness analyses. The dimensional changes during this process was found in another study to be approximately 15.8% [20]. Therefore, the final specimens that are mounted for testing are approximately 15.8% of the original size of detailed in Table 1.

### 3.2 Procedure for microstructural investigation

In this research study, the microstructural and material properties of the process and metal powder used are analyzed in relation to the MME process. When characterizing the feasibility of the process, the correlation between the printing parameters and the resultant porosity provides valuable insight into the properties. The printing parameters for the specimens used in this study are shown in Table 1. MME

During the sintering process, specimens experience extremely high temperatures, and the polymer base material either melts out of the part or sublimates to a gaseous state. This resultant loss of material inevitably results in dimensional and density losses. Through the use of an inverting microscope, the percent area porosity of the specimens can be analyzed post-sintering for the production pores. This analysis allows for the observation of the metal powder bead

bonding and production of vacant spaces. A proper understanding of how the sintering process affects the overall rigidity of the part is necessary to characterize this method as a valid fabrication process. When loaded in tensile, fatigue, or creep, the effects of stress concentration in these cavitations cannot be ignored. However, understanding these effects can lead to design criteria that minimize the reduction in strength and maximize the benefits of this AM technique.

The percent area porosity is defined as the ratio of unoccupied space to occupied space. In the case of microstructural analysis of metal parts, the unoccupied space is the pores resulting from the sintering process, and the occupied space is the region of form metal for a given area. The definition of percent area porosity in relation to the microstructure of copper MME parts is demonstrated in Fig. 5.

Copper specimens of varying printing parameters (Table 1) are sectioned using a diamond disc cutting blade on a SYJ-200 precision cutting saw. For each set of three specimens of correlative printing parameters, a specimen is mounted to expose a XY, Z, and sectioned axis to the microscope. The locations of these examinations are based on the cartesian axes of the printing apparatus, for example the Z-axis refers to the  $z$  printing direction, and are as follows:

- XY—Microstructural porosity was examined/averaged on the cube faces that exposed the layer lines of the printing process and correlate to the XY cartesian printing axes.
- Z—Microstructural porosity was examined/averaged on the cube faces that exposed the top/bottom layers of the printing process and correlate to the Z cartesian printing axes.
- Section—Microstructural porosity was examined/averaged on sectioned cube faces in the center of the specimen.

Each of these samples are mounted using a slow curing epoxy and pulled in a vacuum to eliminate the inclusion of air bubbles. After hardening, the mounted samples are polished and imaged using the following procedure:

**Fig. 5** Description of microstructural percent area porosity, and demonstration of the microstructure of MME parts post-sintering

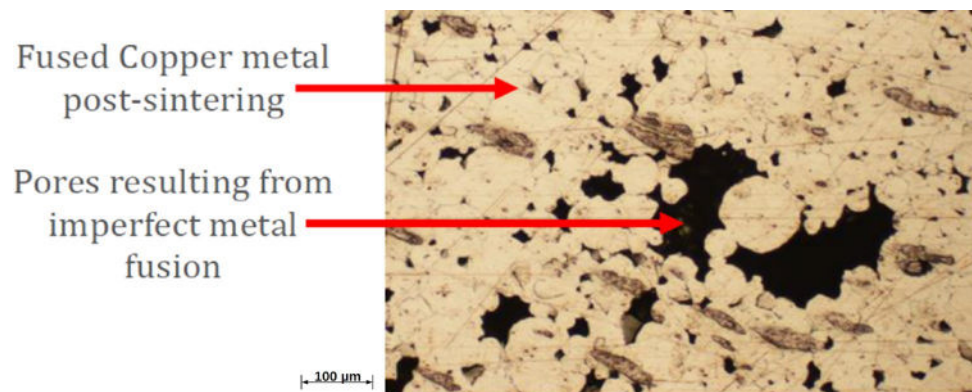


**Table 3** Microstructural analysis results from copper-MME fabricated parts

Microstructural analysis by magnification (averaged from XY, Z, and section views)	10×	20×	40×
Average percent area porosity by magnification	13.19 ± 1.19%	10.83 ± 1.00%	7.19 ± 1.04%
Average total percent area porosity by magnification	10.40 ± 1.74%		
Microstructural analysis by view (averaged from 10×, 20×, 40×)	Section	XY	Z
Average area percent porosity by view	6.18 ± 0.75%	13.13 ± 1.20%	12.52 ± 0.91%
Average total area percent porosity by view	10.61 ± 2.22%		
Total area percent porosity	10.51 ± 1.26%		

- Specimens are polished with emery papers for grits from 400 to 600
- Then the lapping operation is performed using diamond paste of 3 μm and 1 μm grits.
- Final images are taken on a Nikon SMZ 1500

After mounting and polishing the specimens, the porosity is examined at different magnifications and views for the percent area porosity of voids. The microscope software is able to perform image processing and select the percentage of pores for a given area. This tolerance can be selected to not include minor imperfections such as discoloration from polishing compound or scratches from post-processing. The overall results are further shown in Table 3. The total sample size for the analysis of porosity is comprised of 6 samples, 3 magnifications, and 3 mounted views resulting in a total dataset of 54 values.

The microstructural analysis values show a significant amount of fused metal post-sintering with, on a microlevel, the internal structure containing significantly fewer voids. Depending on the application of MME, the 89.44% overall fused material is an acceptable and quantifiable metric with overall percent area trends shown in Figs. 6 and 7.

The average percent area porosity by magnification is 10.40 ± 1.74%; the data are averaged by magnification and do not consider the specimen view bias. The significant difference in percent area porosity between the magnification of 10× and 40× demonstrates that the specimens are mostly comprised of larger pores. Therefore, it can be concluded that the final total average is primarily comprised of larger pores. The average percent area porosity by view is 10.61 ± 2.22%; the data are averaged by view and do not consider the magnification bias. The significantly lower percent area porosity within the section view data when compared to the XY–Z views data demonstrates that the metal is more fully fused in the center of the specimens. Therefore, it can be concluded that a majority of voids within the total average are located at the outer edges of the samples. The total average percent area porosity is approximately 10.51 ± 1.26%. Therefore, the final percent of fused metal based on the microstructure is 89.44 ± 1.26% with a majority

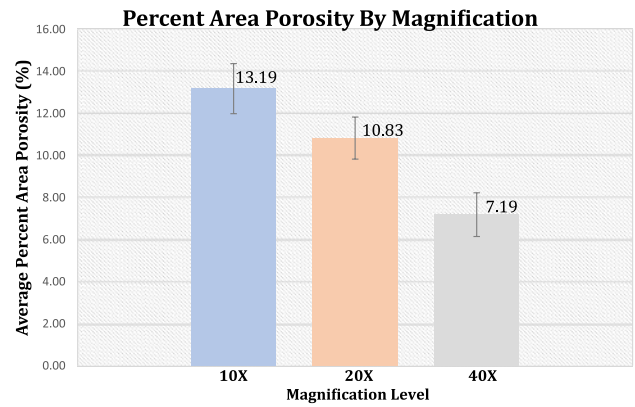


**Fig. 6** Percent area porosity in correlation to examined magnification

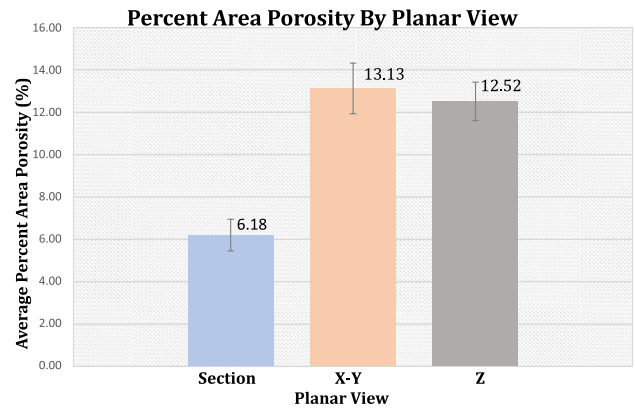


**Fig. 7** Percent area porosity in correlation to the planar view of the specimen

of the resultant porosity from the MME process being larger pores located on the outer edges of the specimens.

### 3.3 Procedure for hardness investigation

The mechanical properties of hardness are analyzed in relation to the MME process. When validating the feasibility of this fabrication method, the mechanical strength

and rigidity are important characteristics to consider when designing for any potentially load-bearing application. The primary material examined in this study is copper MPC with a metal composition of 90% by weight and approximately 65% by volume. The printing parameters are as described in Sect. 3.1, and the specimens are tested using a Rockwell Hardness method.

A reference set of specimens for copper is tested three times on three different samples of copper to establish a valid average. For the experimental setup, a nonconventional Rockwell Hardness test for copper (HRH) is performed so a reference value with the same setup must be used. The MPC material that is used for the MME study is fabricated utilizing powder metallurgy. Therefore, the hardness is expected to be significantly lower. In preliminary testing, the indenter and force load of the standard copper HR tests of HRB and HRF resulted in invalid numbers in the MME specimens. This is due to the fabrication method of powder metallurgy significantly affecting the hardness of the finalized object. To consistently achieve valid numbers, the HR testing method with the largest indenter and lowest load is selected. This method is the HRH standard. The hardness analysis shown in Fig. 8 is done with an H Rockwell Hardness (HRH) testing method, which is set to the conditions of a 1/8" ball indenter and an applied force of 60 kg based on the ASTM standard for hardness of metals [22]. The hardness tester used for this analysis is a Wilson Rockwell Series 2000. The standard HRH value for copper, as per testing, is found to be 106 in a test specimen shown in Fig. 8.

Table 4 demonstrates the hardness data points that are used to formulate an average HRH value for the MME specimens. For reference, the aforementioned test copper was found to have an average HRH value of 106 shown in Fig. 8. This value is used to calculate the percent difference between the reference copper and MME copper fabricated samples for the non-standard HRH testing method for copper.

From the data shown in Table 4, these 18 data points are used to establish an overall average value of  $44.68 \pm 5.66$ . The average variation is quite significant with an error of 5.66 HRH and further evidenced by values of ~ 10 HRH as well as ~ 100 HRH. The significant difference in error demonstrates that the sintering process does not fuse the objects uniformly. The percent difference between the aforementioned standard copper HRH value of 106, and the MME specimen value of 44.68 is approximately 58%. The final conclusion that can be drawn from the data is that for the process of MME there is a hardness loss of greater than 50% when compared to standard copper, and that the hardness of the copper powder does not fuse uniformly.

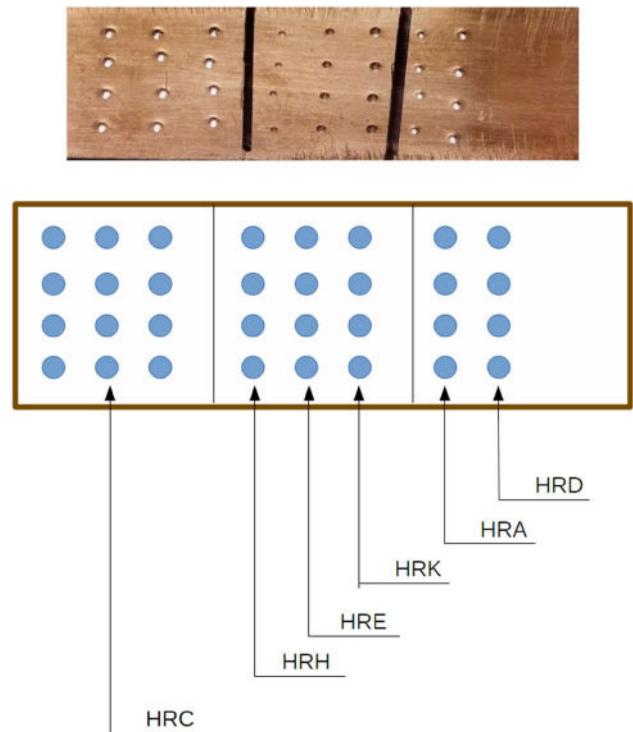


Fig. 8 Copper piece used for a variety of testing methods to better compare MME results

Table 4 HRH hardness values in MME copper

Al <sub>2</sub> O <sub>3</sub> sintering ballast				
Specimen	XY	Z	Sec	Average
CU01510	54.9	42.8	43.9	44.68
CU01520	45.3	8.8	59.7	
CU022510	41.6	48.0		Percent diff:
CU022520	10.8	4.7		57.98%
CU0310	40.2	47.7	96.1	
CU0320	52.3	49.8	68.2	

## 4 Discussion

This research study examines the process of MME, and the influences that printing parameters have on the dimensional, microstructural, and hardness properties. These values are related to the parameters at which the specimens were printed, and the influence of outside variables could be investigated further.

It is shown that the dimensional losses can be mitigated to be as low as 5% under the ideal printing and sintering conditions. For more precise printing parameters, the dimensional losses are lessened. However, as the accuracy decreases, the influence of oxidation on the dimensional

parameters during sintering becomes greater than that of the printing parameters as shown in Fig. 7. This correlation between parameters and dimensional loss is shown to be vague in relation to other variables, such as sintering temperature, time, and ballast type, which can influence the dimensional loss.

For the microstructural data, the internal percent area porosity can also be reduced through printing parameters and sintering material to be as low as 4.3%. As shown in Figs. 6, 7, the percent area porosity of the section view is greatly reduced from the XY and Z views. This difference in the area ratio correlates to greater metal powder bonding in the center of the MME part. Exterior portions of parts fabricated by this method result in great pores, and the interior portions of these parts experience less void production by sintering.

The percent difference between MME specimens and traditionally fabricated parts is a decrease of 58% on the HRH scale when compared to standard copper. The process of PM introduces mechanical properties losses and compensates with the production of complex parts. Likewise, the MME process is shown to be capable of producing complex parts and also introduces mechanical property losses. For a new fabrication method that utilizes the fusion of metal powders, the significant loss of hardness is expected and can be further minimized with future work.

## 5 Conclusions

This study explored dimensional, microstructural, and initial hardness in the MME process. Most powder-based metal printing technologies that utilize sintering do so in a vacuum environment. However, the oxidation effects can be greatly decreased using an inert system. By investigating MME in an open-air environment, it is shown that the dimensional losses can be mitigated to be within an acceptable margin. The ballast that is used and the parameters within which the parts are fabricated all greatly influence the amount of material lost during the sintering procedure. It is further shown that the production of pores on a microstructural level is within an acceptable range, depending on the application. Overall, it is shown that the metal production system developed produces an accurate range of products verified from the dimensional, microstructural, and hardness studies.

**Acknowledgements** This study has been made available through funding by NSF Award 1801120, Smart Manufacturing for America's Revolutionizing Technological Transformation; and NSF Award 1601587, AM-WATCH: Additive Manufacturing—Workforce Advancement Training Coalition and Hub. Editing support provided by Dr. Elizabeth Powell of the Clay N. Hixson Student Success Center and Ms. Amy Hill of the Research Office is greatly appreciated.

## References

1. Wohlers T (2019) Wohlers report 2019: 3D printing and additive manufacturing state of the industry. Wohlers Associates
2. Comb J, Priedeman WR, Turley PW (1994) FDM technology process improvements. Proc. Solid Free. Fabr. Symp., pp 42–49
3. Liang Q-J, Li XD (2018) Application of FDM additive manufacturing technology in making medical surgical model. DEStech Trans. Eng. Technol. Res., no. ecame, pp 133–137
4. Böckin D, Tillman A-M (2019) Environmental assessment of additive manufacturing in the automotive industry. J Clean Prod 226:977–987
5. Wu P, Wang J, Wang X (2016) Automation in Construction A critical review of the use of 3-D printing in the construction industry material Finished. Autom Constr 68:21–31
6. Bos F, Wolfs R, Ahmed Z, Salet T (2016) Additive manufacturing of concrete in construction: potentials and challenges of 3D concrete printing. Virtual Phys Prototyp 11(3):209–225
7. Prater T, Werkheiser MJ, Ledbetter F, Morgan K (2018) In-space manufacturing at NASA Marshall Space Flight Center: a portfolio of fabrication and recycling technology development for the international space station. In: 2018 AIAA Sp. Astronaut. Forum Expo., p 5364
8. Riecker S, Clouse J, Studnitzky T, Andersen O, Kieback B (2016) Fused deposition modeling – opportunities for cheap metal AM. WorldPM2016-AM-Deposition Technologies
9. Gong H, Snelling D, Kardel K, Carrano A (2019) Comparison of stainless steel 316L parts made by FDM- and SLM-based additive manufacturing processes. JOM 71(3):880–885
10. SpaceX (2014) SPACEX launches 3D-printed part to space, creates printed engine chamber. Retrieved 28 Apr 2016
11. Landau E (2014) Printing the metals of the future. NASA, Pasadena
12. EOS (2020) EOS systems. [https://www.eos.info/systems\\_solutions/metal/systems\\_equipment\(online\)](https://www.eos.info/systems_solutions/metal/systems_equipment(online))
13. Frazier WE (2014) Metal additive manufacturing: a review. J Mater Eng Perform 23(6):1917–1928
14. Kuan AY, Hoe-lian D, Rebecca P, Web RP (2016) Metal 3D printing via selective laser melting and direct metal deposition: materials, properties and applications. Prog. Addit. Manuf.
15. Watson J, Vondra H, Fidan I (2018) The development of a framework for 3D printing, casting, and entrepreneurship. In: 2017 ASEE Annual Conference & Exposition Proceedings
16. Fresques T, Cantrell D, Fidan I (2015) The development of a framework between the 3D printed patterns and sand-cast work pieces. Int J Rapid Manuf 5(2):170
17. Duda T, Raghavan LV (2016) 3D metal printing technology. IFAC 49(29):103–110
18. Hwang S, Reyes EI, Sik Moon K, Rumpf RC, Kim NS (2015) Thermo-mechanical characterization of metal/polymer composite filaments and printing parameter study for fused deposition modeling in the 3D printing process. J Electron Mater 44(3):771–777
19. L. The Virtual Foundry (2019) The virtual foundry. <https://www.thevirtualfoundry.com>. Accessed 07 Jul 2019 (online)
20. Terry S, Fidan I, Tantawi K (2019) Dimensional analysis of metal powder infused filament—low cost metal 3D printing. Solid Free. Fabr. Symp. Proc.
21. Terry SM (2019) Innovating the fused filament fabrication process metal powder polylactic acid printing. ProQuest Diss. Publ.
22. ASTM Standard E18 (2015) Standard test methods for rockwell hardness of metallic materials. ASTM International, West Conshohocken, PA, pp 1–38